

# A Fast and Robust Place Recognition Approach for Stereo Visual Odometry using LiDAR Descriptors

Jiawei Mo<sup>1</sup> and Junaed Sattar<sup>2</sup> \*

## Abstract

Place recognition is a core component of Simultaneous Localization and Mapping (SLAM) algorithms. Particularly in visual SLAM systems, a robot must be able to recognize previously-visited places by measuring the appearance similarity between images representing these locations. However, it is sensitive to visual appearance change and also can be computationally expensive. In this paper, we propose an alternative approach that adapts LiDAR descriptors on 3D points obtained from stereo-visual odometry for place recognition. 3D points are more reliable than 2D visual cues (*e.g.*, 2D features) against environmental changes (*e.g.*, variable illumination) which benefits visual SLAM systems in long-term deployment scenarios. Stereo-visual odometry generates 3D points with a consistent scale, which enables us to use global LiDAR descriptors for place recognition with the goal of high computational efficiency. Through extensive evaluations on standard benchmark datasets, we demonstrate the accuracy, efficiency, and robustness of using 3D points for place recognition over 2D methods.

## 1 Introduction

Visual SLAM (**vSLAM**) has been one of the most active research areas in mobile robotics in the past couple of decades. Many field robots, especially where GPS signal reception is weak or unavailable (*e.g.*, in urban or underwater settings), often rely on vision-based systems for navigation. In these systems, visual odometry (VO) is used to build a local map and estimate ego-motion to assist in robot navigation. However, significant error can accumulate throughout the process, which causes odometry estimates to diverge from the correct path. Some form of a “loop closure” approach (*e.g.*, Bag-of-Words [12]) is required to bring non-local constraints into the system to get a globally consistent map and trajectory, which provides a robot the ability to recognize previously-visited

---

\*The authors are with the Department of Computer Science and Engineering, Minnesota Robotics Institute, University of Minnesota Twin Cities, Minneapolis, MN, USA. {<sup>1</sup>mxxx066, <sup>2</sup>junaed} at umn.edu.



(a) Parks Road in spring.



(b) Parks Road in winter.



(c) Holywell Street in spring.



(d) Holywell Street in winter.

Figure 1: RobotCar dataset in different seasons. Note the significant changes in appearance in the two examples shown.

places. Place recognition is thus essential to detect loop closures and improve the accuracy of VO methods.

Classical place recognition methods for vision-based systems usually rely on 2D images. Each location is represented by an image taken at that place. To determine the possibility of two locations being the same place, the similarity of their corresponding images is evaluated. There is extensive literature on image similarity, such as feature Bag-of-Words [12], and GIST [24], which is discussed in Sec. 2.

However, visual odometry methods provide additional information that can be used for place recognition. The depth of points (*i.e.*, the distance of these points from the camera) on 2D images can be partially or fully recovered by monocular or multi-camera visual odometry, respectively. The 3D structure of the scene can potentially provide important information for place recognition; however, 2D place recognition methods ignore this. The 3D structure is more robust than 2D images in a dynamic environment (*e.g.*, under varying illumination). The motivation is also biological, as humans strongly rely on 3D structures for place recognition [9].

On the other hand, a rich body of literature exists on place recognition methods using 3D points from LiDAR (Light Detection and Ranging) sensors. LiDARs scan the 3D structure of the environment, rather than its visual appearance, making LiDAR-based place recognition more robust against environmental changes such as appearance and brightness (*e.g.*, Fig. 1). Another benefit

of LiDAR methods is their high computational efficiency, and our evaluations demonstrate this when comparing 2D image-based and 3D LiDAR methods (see Sec. 4).

In this work, we adapt LiDAR place recognition methods, in particular, LiDAR descriptors, into visual odometry systems for place recognition purposes. The goal is to enable accurate and robust place recognition in a computationally efficient way for a vision-based system in a dynamic environment. *The proposed approach imitates a LiDAR range scan from 3D points generated by stereo-visual odometry, which enables us to adapt global point cloud descriptors.*

Several challenges must be overcome for applying LiDAR-based methods to vision-based systems. First, the 3D points generated by visual odometry are distributed in a “pyramid-like” shape due to the much narrower field-of-view of cameras (excluding omnidirectional cameras) compared to most LiDARs. The pose of the pyramid changes with the camera, which is not desirable for place recognition. The second challenge is how to (and even if it is necessary to) adapt grayscale intensity data from the vision-based system into LiDAR-based methods, as such information is not available to LiDAR sensors. We address these challenges in this work.

To the best of our knowledge, this is the first approach that uses global LiDAR descriptors for place recognition in vSLAM systems. The main contributions of this work, as discussed in Sec. 3, are as follows:

- Adapting global LiDAR descriptors to a vision-based system for place recognition,
- Achieving high accuracy and robustness against visual appearance changes,
- Achieving lower computational cost over existing approaches.

We evaluate the proposed method on the KITTI dataset [14] and the Oxford RobotCar dataset [20]. We demonstrate the robustness of our method against drastic visual appearance change across seasons as recorded in the RobotCar dataset, and do so with high accuracy and computational efficiency over existing methods. Further performance improvement is achieved by augmenting the LiDAR descriptor with grayscale intensity information.

## 2 Related Work

In the field of vSLAM, ORB-SLAM2 [23] is a recent development that demonstrates high accuracy and computational efficiency. In ORB-SLAM2, loop closure is detected by Bag-of-Words (BoW) using ORB features [26]. Place recognition is based on the repeatability of 2D features on images. A vocabulary tree is used in BoW to speed up feature matching and subsequent place queries. BoW works perfectly for ORB-SLAM2 since the feature repeatability is also important and handled by ORB-SLAM2. However, since BoW depends on feature matching, it fails when the features are highly repetitive. An example is given in Fig.

5. LSD-SLAM [8] adopts FAB-MAP [6] (a variant of BoW) for place recognition, which puts lower weights to highly repetitive features to solve the problem mentioned above. Other than BoW, Fisher vectors [25] and VLAD [17] also focus on 2D features. Recently, researchers replaced hand-crafted features (*e.g.*, ORB) with learned features and achieved better performance (*e.g.*, NetVLAD [1] and [3]). On the other hand, global image descriptors are also used to decide the similarity between images for place recognition. GIST [24] is one example, which encodes spatial layout properties (spatial frequencies) of the scene. It exhibits high accuracy if the viewing angle does not significantly change.

Neither BoW or GIST is robust against visual appearance change, which is not ideal for long term (*e.g.*, from summer to winter) vSLAM applications. And both of them are computationally expensive. In ORB-SLAM2, place recognition runs at a separate thread of execution to achieve real-time performance. Direct vSLAM systems (*e.g.*, [7], [11]) have become popular in the past decade, which achieve higher performance in certain scenarios. Adapting BoW into direct vSLAM systems is challenging because feature repeatability is not focused on in these systems. In LSD-SLAM mentioned above, repeatable features are detected and matched separately which are used specifically for place recognition. In LDSO [13], the point selection strategy of a direct vSLAM system is tuned to favor repeatable features to enable BoW. The proposed approach for place recognition in this paper, however, is a more elegant approach for direct vSLAM systems.

A number of 3D place recognition methods have been designed for RGB-D cameras or LiDARs. RGB-D Mapping [16] uses ICP [2] to detect loop closure and RANSAC [10] to get an initial pose for ICP. For LiDARs, place recognition methods can be categorized into local descriptors and global descriptors. *Local descriptors* use a subset of the points and describe them in a local neighborhood. Examples are Spin Image [18] and SHOT [28]. Spin Image describes a keypoint by a histogram of points lying in each bin of a vertical cylinder centered at that keypoint. SHOT creates a sphere around a keypoint and describes that keypoint by the histogram of normal angles in each bin in the sphere. *Global methods* describe the entire set of points. These methods are more computationally efficient; however, they require the scale of the 3D points to be consistent. Recent development includes NDT [21], M2DP [15], Scan Context [19], and DELIGHT [5]. NDT classifies keypoints into line, plane, and sphere classes according to their neighborhoods. A histogram of these three classes is created to represent the point cloud. M2DP projects points onto multiple planes, the histogram of point count in each bin of projection plane is concatenated to get a signature of the point cloud. Scan Context aligns the point cloud to the vertical direction and represents it by the histogram of the maximal height of each bin on the horizontal plane. DELIGHT focuses on LiDAR intensity; the scan sphere is divided into 16 parts and the histogram of LiDAR intensity in each part is calculated to represent the point cloud.

Cieslewski et. al. [4] looked into the possibility of using the 3D points triangulated from Structure-from-Motion or vSLAM for place recognition. They proposed the NBLD descriptor [4] for the 3D points. A keypoint is described

by the neighborhood points in a vertical cylinder. The point density of each bin in the cylinder is calculated, which is then compared with the neighborhood to create a binary descriptor of that keypoint. Ye et. al. [29] extended NBLD with a neural network. The vertical cylinder of NBLD is created in the same way; however, a neural network is used to describe the cylinder, instead of calculating the point density. These are novel approaches in adopting local point cloud descriptors into vision-based systems for place recognition.

In this work, we adapt global LiDAR descriptors into stereo-visual odometry for robust and efficient place recognition under visual appearance change. Direct vSLAM systems can easily adopt the proposed approach for place recognition since feature repeatability is no longer necessary.

### 3 Methodology

Similar to the idea of [4], our method recognizes places based on the 3D points generated by visual odometry. The main difference is that the visual odometry in this work is running on stereo cameras. Specifically, we use SO-DSO [22] as our stereo-visual odometry for its high accuracy and computational efficiency. To the best of our knowledge, SO-DSO is the only fully direct stereo-visual odometry that is independent of feature repeatability. We choose SO-DSO to demonstrate that the proposed method works for direct vSLAM systems. However, any multi-camera visual odometry is applicable here. Since the 3D points generated by stereo-visual odometry have a consistent scale, it is possible to describe them using global LiDAR descriptors, rather than local descriptors [4]. The goal is high accuracy and computational efficiency, and robustness to environmental change.

#### 3.1 Point Cloud Preprocessing

Due to the narrow field-of-view of the cameras, the 3D points generated by stereo-visual odometry are located in a pyramid shape with the vertex of this pyramid being at the focal point. The NBLD local descriptor can operate directly in the pyramid shape, as NBLD describes 3D points individually. However, if we apply a global descriptor directly inside the pyramid shape, place recognition will be very sensitive to the viewing angle.

To solve the issue, we propose *a simple but effective method that transforms pyramid-shaped 3D points from stereo-visual odometry to omnidirectional LiDAR-shaped (spherical) 3D points*. The proposed method is illustrated in Fig. 3. Stereo-visual odometry generates keyframes with camera poses and associated 3D points. We maintain what we refer to as a *local points* list. For each incoming keyframe, we store all its *3D points* into the list. To imitate a LiDAR scan for the current keyframe, we iterate through the *local points* list: if the distance of the point is within the desired LiDAR range, we transform it to the current keyframe coordinate by *current pose*, then put it to the *spherical points* list. Here we assume the camera motion is predominantly in the

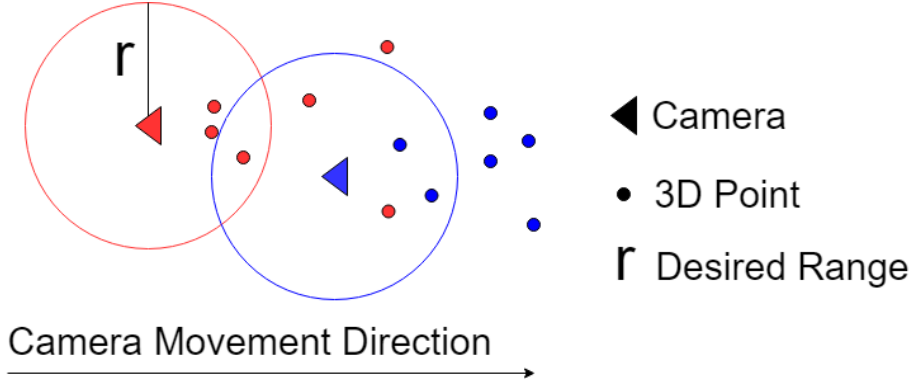


Figure 2: A demonstration of the points generated by visual odometry, with different colors representing different keyframes. 3D points are coming into the desired range as the camera moves.

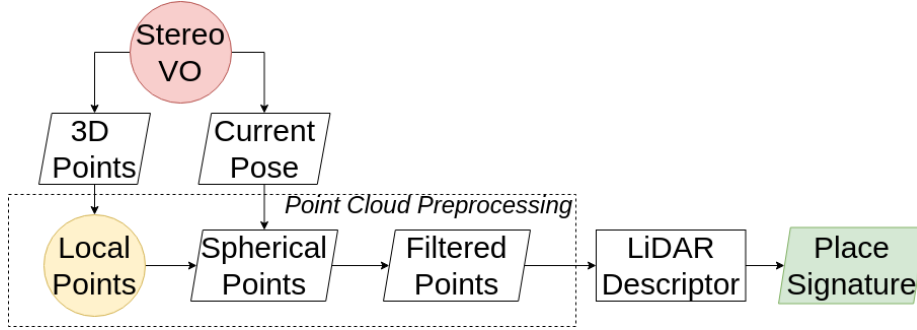


Figure 3: An overview of the proposed approach. The basis lies in the “Point Cloud Preprocessing” block, where 3D points obtained by stereo VO are used to imitate a LiDAR scan, so that efficient place recognition can be performed.

forward direction so that we continuously have points coming into the desired range to compensate for points leaving the range, as illustrated in Fig. 2. The *spherical points* may contain duplicate points; for robustness and computational efficiency, we filter them and get the final *filtered points*.

Caching local points enables us to imitate LiDAR scans with denser omnidirectional points. Since visual odometry generates locally accurate camera poses and 3D points, concatenating 3D points transformed from multiple nearby keyframes to imitate a LiDAR scan is feasible.

### 3.2 Point Cloud Description

The next step in the proposed method is to describe the *filtered points* and get a *place signature* for the keyframe, for which we rely on global descriptors. This is preferable for two reasons: the first is for its computational efficiency when describing and matching the point clouds; secondly, since the point clouds we

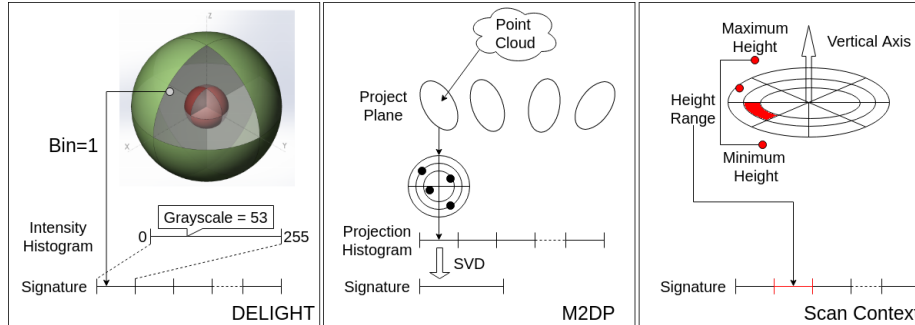


Figure 4: A demonstration of LiDAR descriptors used in this work: DELIGHT, M2DP, and Scan Context.

have are generated by visual odometry, they are not as consistent and dense as the ones from a LiDAR. Many local descriptors, such as Spin Image, depend on the surface normal for which dense point clouds are required, which would be problematic in this case. We choose DELIGHT [5], M2DP [15], and Scan Context [19] as our global descriptors since they are state-of-the-art LiDAR descriptors for place recognition that are robust to sparse and inconsistent point clouds. The high-level ideas of them are illustrated in Fig. 4.

**DELIGHT** DELIGHT operates on LiDAR intensities. The LiDAR scan sphere is divided into 16 bins by radius, azimuth, and elevation. Each bin is described by the histogram of LiDAR intensities inside, which are concatenated to form the signature representing the entire LiDAR scan. To make the descriptor less sensitive to rotation and translation, the raw LiDAR scan is aligned to a reference frame obtained by Principal Components Analysis (PCA) [27]. As discussed in [5], there are four versions of the signatures due to the ambiguity of PCA.

Analogous to LiDAR scan intensities, the 3D points from the visual odometry have grayscale intensities. We simply replace LiDAR intensities with grayscale intensities and adapt the DELIGHT descriptor into our system. Each histogram is composed of 256 bins since the grayscale intensity ranges from 0 to 255. Although DELIGHT does not use 3D structural information, we include it in this work to contrast it against M2DP and Scan Context as both these methods use this information. This is done to highlight the value of 3D structures for robust place recognition against visual appearance change.

**M2DP** M2DP is a global descriptor that demonstrates high accuracy and efficiency. The point cloud is projected onto multiple planes, each plane is separated into individual bins by radius and azimuth. The distribution of projection onto bins are concatenated to form a signature for the point cloud. For computational and memory efficiency, singular-value decomposition (SVD) is used to compress the signature. As in DELIGHT, PCA is used to align the point cloud.

In this work, we augment the M2DP descriptor using grayscale intensity from the visual odometry. Specifically, when projecting the point cloud onto each plane, we not only count the number of points projected onto each bin but also calculate the average grayscale intensity. Therefore, we have two types of signatures (namely point count signature and intensity signature) for each place. To make the intensity signature less sensitive to illumination, we binarize the intensity by comparing it to the global average intensity. The intuition is to highlight the bright bins. To improve accuracy, we adopt the four versions of signature from DELIGHT. We include M2DP in our method as it utilizes 3D structure for place recognition and is not limited to urban scenarios like Scan Context.

**Scan Context** Scan Context is a straightforward yet effective descriptor designed for LiDAR scans obtained in urban areas. The LiDAR scan is aligned with respect to the gravitational axis which is measured externally (*e.g.*, with an IMU). Then the horizontal circle plane is separated into multiple bins by radius and azimuth. In each bin, the maximum height is found and concatenated to form a signature for the current place.

To fit Scan Context into our system, we make the following modifications. First, since we want to avoid using additional sensors, we adopt the PCA method used in DELIGHT and M2DP to align the point cloud vertically. Second, due to the PCA ambiguity, we replace maximum height with height range (maximum height - minimum height). Lastly, we generate the intensity signature as in the modified M2DP. Scan Context is the most efficient and accurate among the three descriptors, as shown in experimental evaluations (Sec. 4).

### 3.3 Place Recognition

Using the place signatures, we are able to determine the similarity between places. We generate a **difference matrix** by calculating the signature distance from each query place to every place in the reference database. For DELIGHT and M2DP, we take the shortest distance from the query signature to all four possible signatures of the reference place. For Scan Context, we take the shortest distance against all possible yaw angles since we align the point cloud vertically by PCA. The distance of DELIGHT is based on the chi-squared test as described in [5]. For M2DP and Scan Context, the distance is simply the Euclidean distance between normalized (L2-norm=1) signatures. As we have two types of signatures (structure signature and intensity signature), we get two individual difference matrices  $\mathbf{D}_s$  and  $\mathbf{D}_i$ . We fuse them in Eq. 1 by normalizing (mean=0, std=1) each row (representing each query) and adding them with a relative weight  $w_s$ :

$$\mathbf{D}_{\text{fused}} = \frac{w_s \cdot N_{\text{row}}(\mathbf{D}_s) + N_{\text{row}}(\mathbf{D}_i)}{w_s + 1} \quad (1)$$

With the difference matrix, each query place (row) is matched to the reference place with the least difference value among all candidates (along the



row).

## 4 Experimental Evaluation

To evaluate the proposed method, we compare the results internally among DELIGHT, M2DP, and Scan Context, as well as externally to BoW, GIST, and [29].

### Implementation

We use the fast (less accurate) setting ( $\leq 800$  active points,  $\leq 6$  frames in optimization) of SO-DSO to estimate camera poses and generate 3D points. We found that the fast setting is good enough for our purpose and introducing more points decreases the computational efficiency. The outputs of SO-DSO (poses and points) are used by the proposed methods for place recognition.

The authors of M2DP have published their Matlab code, which we re-implement using C++. We similarly re-implement DELIGHT and Scan Context. When preprocessing the point cloud as discussed in Sec. 3.1, we set LiDAR range  $r = 45.0m$ . For DELIGHT and M2DP, spherical points are filtered in polar coordinate with 1-degree angular resolution. We keep the closest point along each ray originating from the polar center. For Scan Context, however, we filter points in the Cartesian coordinate with  $1.5m \times 0.75m \times 1.5m$  resolution. We switch to the Cartesian coordinate and assign a higher resolution along the vertical axis because Scan Context focuses on height. For the KITTI dataset [14], there are 2706.2 (1610.6) points on average in each *filtered points* using polar (Cartesian) filtering. For DELIGHT, the radius of the inner/outer sphere is set to 10/45 meters, respectively. The parameters of M2DP and Scan Context are set to default values. For more details, our implementations are available online<sup>1</sup>. When fusing difference matrices in Eq. 1, we set higher weight  $w_s = 2$  to structure because structure is more reliable than grayscale intensity.

The implementation of BoW comes from ORB-SLAM2; the implementation of GIST is available online<sup>2</sup>. No implementation of [29] was available, so we use the same experimental setup for fair comparison.

### Evaluation

For place recognition accuracy, we focus on the area under the precision-recall curve (**AUC**) and the maximal recall at 100% precision (no false positives, *i.e.*, no errors) as two indices. Larger AUC means more places are recognized with fewer errors. To some extent, AUC reflects the discrimination power of an algorithm for place recognition. Larger maximal recall at 100% precision indicates that more places are recognized before making any mistakes, it is important because a single false positive might significantly affect the accuracy of the entire

---

<sup>1</sup>[https://github.com/jiawei-mo/so\\_dso\\_place\\_recognition](https://github.com/jiawei-mo/so_dso_place_recognition)

<sup>2</sup><http://lear.inrialpes.fr/software>

Method	DELI.	M2DP	S.C.	BoW	GIST
Seq. 00	0.754 0.616	0.639 0.191	0.733 0.599	<b>0.893 0.788</b>	0.841 0.774
Seq. 02	0.463 0.253	0.488 0.053	0.555 0.440	0.011 0.012	<b>0.613 0.597</b>
Seq. 05	0.622 0.483	0.522 0.062	0.653 0.566	<b>0.867 0.809</b>	0.756 0.659
Seq. 06	0.916 0.531	0.946 0.671	0.897 0.679	<b>0.968 0.963</b>	0.925 0.729
Seq. 07	0.000 0.000	0.000 0.000	0.000 0.000	<b>0.713 0.627</b>	0.350 0.149

Table 1: AUC (first number) and maximal recall at 100% precision (second number) on KITTI dataset.



Figure 5: Snapshot of KITTI seq. 02 at a revisited place.

SLAM algorithm. In the ideal case, both AUC and maximal recall should be 1. Other than accuracy, computational efficiency is also evaluated. We take apart each algorithm and compare the components individually. The accuracy and efficiency are evaluated on KITTI dataset [14] and Oxford RobotCar Dataset [20].

## KITTI Dataset

The KITTI dataset is one of the most influential datasets for benchmarking autonomous driving research. The odometry dataset comes with 22 stereo sequences. However, only the first 11 sequences have ground-truth publicly available. Among them, sequences {00, 02, 05, 06, 07} have loop closure segments, which are used in this section.

**Accuracy** When computing precision and recall, two places are considered to be revisited places if their distance is smaller than 10 meters. As the internal distance of trajectories in the KITTI dataset can be small (*e.g.*, sequence 06 in Figure 6), we set a relatively small threshold to avoid false positive in the ground-truth.

Table 1 reports the accuracy of each algorithm. BoW achieves the best accuracy in all sequences other than sequence 02. Each sequence in the KITTI dataset is recorded continuously in a short period of time, there is not much visual appearance change. Hence, feature matching is robust and BoW works perfectly. For sequence 02, the BoW approach fails to recognize places because the revisited places are occupied with repetitive textures (*i.e.*, plants in Fig. 5), for which feature matching is unreliable. The accuracy of the adapted LiDAR

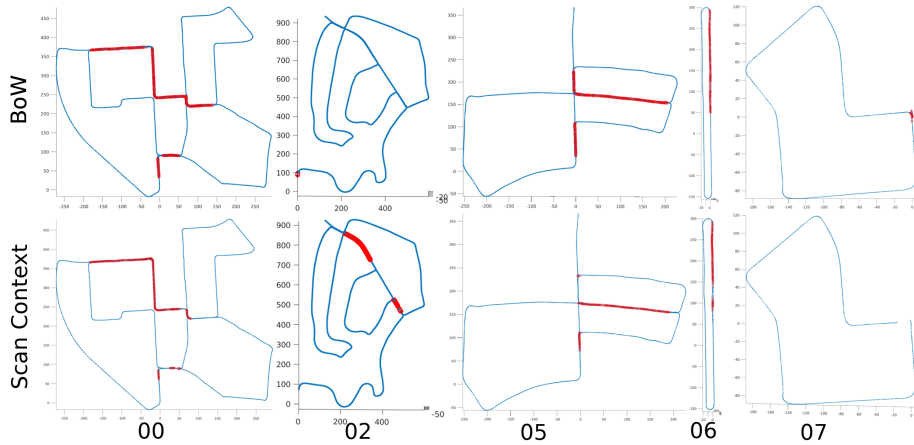


Figure 6: Places recognized (marked as red) by BoW and by Scan Context on KITTI dataset at 100% precision.

Method	DELI	M2DP	S.C.	BoW	GIST
Imitate LiDAR Scan (c++)	1.151	1.204	<b>0.692</b>	-	-
Desc. extraction (c++)	<b>0.082</b>	46.10	0.123	37.41	160.0
Query descriptor (Matlab)	103.2	3.418	7.334	115.0	<b>1.106</b>
Total	104.4	50.72	<b>8.149</b>	152.4	161.1

Table 2: Run time analysis in milliseconds.

approaches is not as good as BoW or GIST but their AUCs are still fairly high on sequences  $\{00, 02, 05, 06\}$ . Scan Context achieves the best overall accuracy among the adapted LiDAR approaches. Sequence 07 is special because there is only a small segment of loop closure when the vehicle comes back to the starting place. Thus, the accuracy of BoW and GIST is not very reliable. None of the proposed 3D methods detects any loop because there is not enough overlapped trajectory.

Figure 6 plots the loops detected by BoW and Scan Context. Scan Context fails to recognize places in short segments. This is because the proposed method needs enough overlapped trajectory to accumulate local points. This is a limitation of the proposed method. But it recognized places with repetitive textures in sequence 2. Nevertheless, we showed that our implementation of each algorithm works on the KITTI dataset (at least for BoW and GIST, we will further validate the proposed 3D approaches using the RobotCar dataset).

**Efficiency** Table 2 reports the run-time required to query a place in the database. The test platform is based on an Intel i7-6700 with 16GB of RAM. The run-time is calculated on Sequence 06 with 880 places (keyframes).

Point filtering in Scan Context is slightly faster because of simple Cartesian

Tests	Spr. Spr.	Spr. Sum.	Spr. Fall	Spr. Win.	Sum. Sum.	Sum. Fall	Sum. Win.	Fall Fall	Fall Win.	Win. Win.
Dates	05-19 05-22	05-19 08-13	05-19 10-30	05-19 02-10	08-13 07-14	08-13 10-30	08-13 02-10	10-30 11-28	10-30 02-10	02-10 12-12

Table 3: Test sequences on RobotCar dataset.

coordinate filtering. For descriptor generation, DELIGHT is the fastest due to its straightforward mechanism. Scan Context is the second-fastest because calculating the height range is also efficient. M2DP is the slowest one among all adapted 3D methods. The entire set of points is projected onto multiple planes, followed by SVD compression, which is computationally expensive. For BoW and GIST, their high accuracy on the KITTI dataset is achieved at a high computational cost. For place query, GIST is the quickest since it simply calculates the Euclidean distance between two descriptors. This is followed by M2DP, for which we have calculated all four descriptors of each place, the distance between two places is simply the smallest Euclidean distance. Scan Context is slightly slower because the query descriptor is matched against all possible yaw. DELIGHT and BoW are much slower since the distances are based on the chi-squared test and L1 norm, respectively.

Scan Context achieves the highest overall efficiency that can run in real-time in most vSLAM systems. Although BoW and GIST achieve higher accuracy, they are much slower than Scan Context.

## RobotCar Dataset

RobotCar dataset is challenging for place recognition since visual appearance and brightness changes drastically. Snapshots of RobotCar are shown in Fig. 1. The testing pairs are given in Table 3, covering all combination of seasons.

**Accuracy** Since the authors of [29] have not published their code, we evaluate our algorithms using the same settings for fair comparisons. Specifically, we use the same segment as illustrated in Fig. 5(a) of [29] for testing. When computing precision and recall, we also use 25 meters as the GPS distance threshold.

Table 4a shows the AUC of each algorithm running the tests in Table 3. Data of [29], NBLD, and NetVLAD are taken directly from [29], whereas rows marked “DELI.”, “M2DP”, and “S.C.” represent our approaches adapting these three global descriptors. Table 4b illustrates the maximal recall with 100% precision. Scan Context (“S.C.”) achieves both the highest AUC and the highest recall in most tests. Scan Context depends on the height range for place recognition. In the RobotCar dataset, the maximum/minimum height is usually from buildings/ground. Therefore, the height range is not very sensitive to season change. GIST behaves best in the rest of the tests. It works well because the viewing angle is mostly unchanged in the RobotCar dataset. M2DP is the next-best performing approach, which has relatively high accuracy when there is less visual appearance change (*e.g.*, *Test a*: Spring-Spring). However, in different

Tests	Spr. Spr.	Spr. Sum.	Spr. Fall	Spr. Win.	Sum. Sum.	Sum. Fall	Sum. Win.	Fall Fall	Fall Win.	Win. Win.
[29]	0.774	0.736	0.589	0.419	0.764	0.557	0.489	0.599	0.443	0.597
NBLD	0.651	0.700	0.611	0.351	0.672	0.496	0.379	0.454	0.351	0.491
NetV.	0.482	0.583	0.427	0.537	0.640	0.259	0.512	0.003	0.078	0.158
DELI.	0.869	0.677	0.445	0.040	0.836	0.612	0.008	0.498	0.003	0.014
M2DP	0.900	0.851	0.498	0.322	0.853	0.519	0.276	0.540	0.349	0.541
S.C.	<b>0.956</b>	<b>0.944</b>	<b>0.782</b>	0.729	<b>0.928</b>	<b>0.779</b>	0.618	<b>0.644</b>	0.491	<b>0.814</b>
BoW	0.558	0.342	0.208	0.300	0.305	0.418	0.371	0.002	0.293	0.001
GIST	0.932	0.918	0.679	<b>0.778</b>	0.914	0.694	<b>0.738</b>	0.003	<b>0.606</b>	0.000

(a) AUC.

Tests	Spr. Spr.	Spr. Sum.	Spr. Fall	Spr. Win.	Sum. Sum.	Sum. Fall	Sum. Win.	Fall Fall	Fall Win.	Win. Win.
DELI.	0.334	0.070	0.026	0.000	0.434	0.187	0.000	0.055	0.000	0.008
M2DP	0.302	0.232	0.001	0.010	0.032	0.011	0.058	0.117	0.039	0.013
S.C.	0.758	<b>0.558</b>	<b>0.408</b>	<b>0.322</b>	<b>0.685</b>	<b>0.415</b>	<b>0.325</b>	<b>0.346</b>	<b>0.247</b>	<b>0.519</b>
BoW	0.032	0.021	0.023	0.031	0.005	0.034	0.100	0.000	0.043	0.000
GIST	<b>0.794</b>	0.377	0.242	0.176	0.503	0.242	0.156	0.000	0.109	0.000

(b) Maximal recall at 100% precision.

Table 4: Place recognition accuracy on RobotCar dataset.

seasons, the trees along the streets have vastly different appearances (*e.g.*, for losing leaves) as illustrated in Fig. 1. M2DP projects all 3D points to get a signature, so its accuracy drops. DELIGHT suffers more from visual appearance change between seasons because it purely depends on grayscale intensity, which indicates the importance of 3D structure for place recognition. BoW has the worst performance, the potential reason is that feature matching is sensitive to changing scene factors such as trees and vehicular (and pedestrian) traffic.

Fig. 7 shows the places recognized by Scan Context at 100% precision. For the easy case (Spring-Spring), Scan Context recognizes most of the places. For the challenging case (Spring-Winter), with the reference of Fig. 1, most places along Holywell street are correctly recognized since it is occupied mostly with buildings; but most places along Parks road are not recognized because there are many trees (maximum height) on both sides of the road.

Fig. 8 shows the decrease in accuracy of each algorithm with seasonal visual appearance change. For AUC, Scan Context and GIST outperform the rest in terms of robustness; for maximal recall, BoW has an abnormal curve because all of its maximal recall values are very low (Table 4b). Other than that, Scan Context is the most robust one. Therefore, we conclude that Scan Context is robust against visual appearance change.

Fig. 9 shows the comparison of the precision-recall curve between the adapted Scan Context and the methods proposed in [29]. It validates that Scan Context adapted in this work outperforms [29] in accuracy.

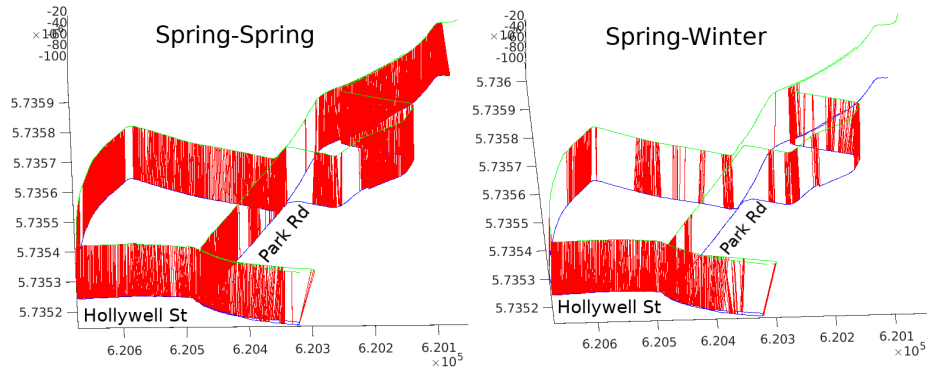


Figure 7: Places recognized (marked as red) by Scan Context at 100% precision.

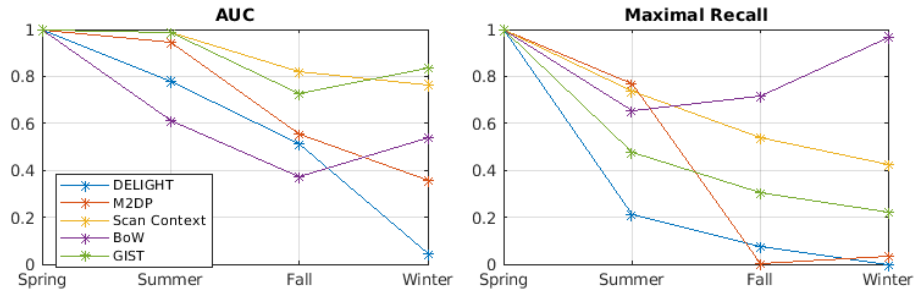


Figure 8: Robustness against seasonal visual appearance change. Using spring as query season. Values are normalized by Spring-Spring.

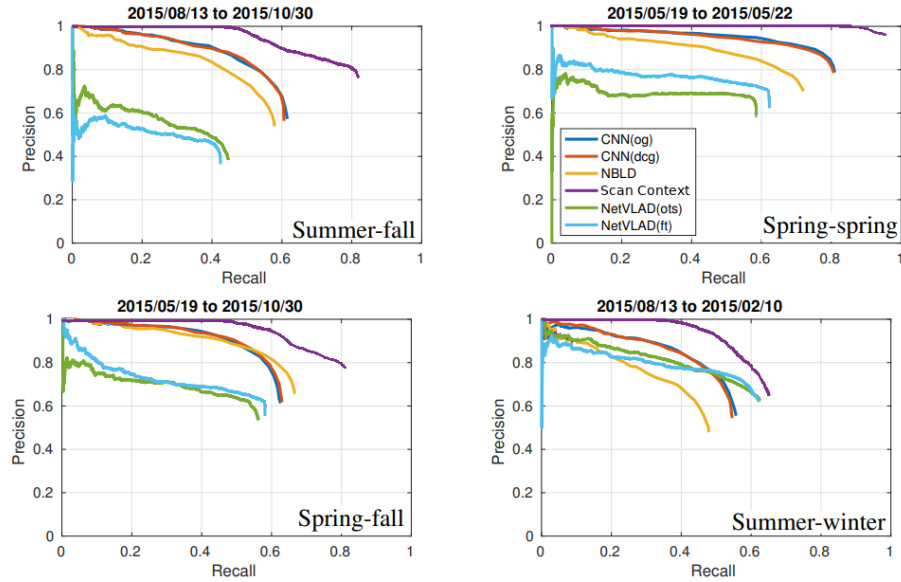


Figure 9: Precision-recall curves of Scan Context compared with that of [29].

Tests	Spr. Spr.	Spr. Sum.	Spr. Fall	Spr. Win.	Sum. Sum.	Sum. Fall	Sum. Win.	Fall Fall	Fall Win.	Win. Win.
Structure	0.955 0.270	0.940 0.216	0.762 0.390	0.699 0.154	<b>0.931</b> 0.279	0.753 0.066	0.610 0.105	<b>0.652</b> 0.147	<b>0.500</b> 0.049	0.778 0.134
Intensity	0.834 0.230	0.645 0.050	0.344 0.039	0.112 0.021	0.831 0.151	0.390 0.057	0.086 0.027	0.290 0.056	0.096 0.027	0.478 0.032
Fused	<b>0.956</b> <b>0.758</b>	<b>0.944</b> <b>0.558</b>	<b>0.782</b> <b>0.408</b>	<b>0.729</b> <b>0.322</b>	0.928 <b>0.685</b>	<b>0.779</b> <b>0.415</b>	<b>0.681</b> <b>0.325</b>	0.644 <b>0.346</b>	0.491 <b>0.247</b>	<b>0.814</b> <b>0.519</b>

Table 5: AUC (top sub-rows) and maximal recall (bottom sub-rows) at 100% precision of Scan Context with structure and/or grayscale intensity.

**Intensity Contribution** Table 5 shows the AUC and maximal recall of Scan Context using structure only, intensity only, and both structure and intensity. Scan Context with intensity only performs poorly on the RobotCar dataset, since grayscale intensity changes drastically throughout different seasons. However, augmenting the structure descriptor with intensity information clearly improves the maximal recall, even though it does not obviously improve the AUC.

We do not include the efficiency comparison on the RobotCar dataset since we use the identical setup with the KITTI dataset and the results are similar.

## Use Case Analysis

After the experiments, we claim that the use case of the proposed method is for forward-moving vehicles (*e.g.*, cars) with intensive visual appearance change (*e.g.*, RobotCar dataset), where the proposed approach recognizes place with high accuracy, efficiency, and robustness. It also works with repetitive texture (*e.g.*, Sequence 02 of KITTI dataset). For direct vSLAM (*e.g.*, DSO [7]), adopting the proposed approach is easier than adopting BoW.

The conventional BoW works on individual images, there is no forward-moving constraint. It achieves higher accuracy especially for small loop segments (*e.g.*, Fig. 6) when there is not much visual appearance change.

## 5 Conclusions

In this paper, we propose a novel place recognition approach for stereo-visual odometry. Instead of 2D image similarity, we depend on the 3D points generated by the visual odometry to determine the correlation between places. The 3D points from stereo systems, with accurate and consistent scale, are used to imitate LiDAR scans and fed into three global LiDAR descriptors, which are DELIGHT, M2DP, and Scan Context. We augment the descriptors with grayscale intensity information. Experiments on the KITTI dataset and RobotCar dataset show the accuracy, efficiency, and robustness of the proposed method.

For the next step, we will integrate the proposed method into state-of-the-art stereo-visual odometry algorithms to detect loop closure, and quantify the performance and accuracy. Furthermore, we intend to implement the proposed algorithm on board physical field robots and validate its performance in visually challenging environments.

## References

- [1] Relja Arandjelovic, Petr Gronat, Akihiko Torii, Tomas Pajdla, and Josef Sivic. NetVLAD: CNN Architecture for Weakly Supervised Place Recognition. In *Proceedings of the IEEE Conference on Computer Vision and Pattern Recognition*, pages 5297–5307, 2016.
- [2] Paul J Besl and Neil D McKay. Method for Registration of 3-D Shapes. In *Sensor Fusion IV: Control Paradigms and Data Structures*, volume 1611, pages 586–607. International Society for Optics and Photonics, 1992.
- [3] Zetao Chen, Adam Jacobson, Niko Sünderhauf, Ben Upcroft, Lingqiao Liu, Chunhua Shen, Ian Reid, and Michael Milford. Deep Learning Features at Scale for Visual Place Recognition. In *2017 IEEE International Conference on Robotics and Automation (ICRA)*, pages 3223–3230. IEEE, 2017.
- [4] Titus Cieslewski, Elena Stumm, Abel Gawel, Mike Bosse, Simon Lynen, and Roland Siegwart. Point Cloud Descriptors for Place Recognition using Sparse Visual Information. In *2016 IEEE International Conference on Robotics and Automation (ICRA)*, pages 4830–4836. IEEE, 2016.
- [5] Konrad P Cop, Paulo VK Borges, and Renaud Dubé. DELIGHT: An Efficient Descriptor for Global Localisation using LiDAR Intensities. In *2018 IEEE International Conference on Robotics and Automation (ICRA)*, pages 3653–3660. IEEE, 2018.
- [6] Mark Cummins and Paul Newman. FAB-MAP: Probabilistic Localization and Mapping in the Space of Appearance. *The International Journal of Robotics Research*, 27(6):647–665, 2008.
- [7] Jakob Engel, Vladlen Koltun, and Daniel Cremers. Direct Sparse Odometry. *IEEE transactions on pattern analysis and machine intelligence*, 40(3):611–625, 2017.
- [8] Jakob Engel, Thomas Schöps, and Daniel Cremers. LSD-SLAM: Large-Scale Direct Monocular SLAM. In *European conference on computer vision*, pages 834–849. Springer, 2014.
- [9] Russell Epstein and Nancy Kanwisher. A Cortical Representation of the Local Visual Environment. *Nature*, 392(6676):598, 1998.



- [10] Martin A Fischler and Robert C Bolles. Random Sample Consensus: A Paradigm for Model Fitting with Applications to Image Analysis and Automated Cartography. *Communications of the ACM*, 24(6):381–395, 1981.
- [11] Christian Forster, Matia Pizzoli, and Davide Scaramuzza. Svo: Fast semi-direct monocular visual odometry. In *2014 IEEE international conference on robotics and automation (ICRA)*, pages 15–22. IEEE, 2014.
- [12] Dorian Gálvez-López and Juan D Tardos. Bags of Binary Words for Fast Place Recognition in Image Sequences. *IEEE Transactions on Robotics*, 28(5):1188–1197, 2012.
- [13] Xiang Gao, Rui Wang, Nikolaus Demmel, and Daniel Cremers. Ldso: Direct sparse odometry with loop closure. In *2018 IEEE/RSJ International Conference on Intelligent Robots and Systems (IROS)*, pages 2198–2204. IEEE, 2018.
- [14] Andreas Geiger, Philip Lenz, Christoph Stiller, and Raquel Urtasun. Vision meets robotics: The kitti dataset. *The International Journal of Robotics Research*, 32(11):1231–1237, 2013.
- [15] Li He, Xiaolong Wang, and Hong Zhang. M2DP: A Novel 3D Point Cloud Descriptor and its Application in Loop Closure Detection. In *2016 IEEE/RSJ International Conference on Intelligent Robots and Systems (IROS)*, pages 231–237. IEEE, 2016.
- [16] Peter Henry, Michael Krainin, Evan Herbst, Xiaofeng Ren, and Dieter Fox. RGB-D mapping: Using Kinect-Style Depth Cameras for Dense 3D Modeling of Indoor Environments. *The International Journal of Robotics Research*, 31(5):647–663, 2012.
- [17] Hervé Jégou, Matthijs Douze, Cordelia Schmid, and Patrick Pérez. Aggregating Local Descriptors into a Compact Image Representation. In *CVPR 2010-23rd IEEE Conference on Computer Vision & Pattern Recognition*, pages 3304–3311. IEEE Computer Society, 2010.
- [18] Andrew E. Johnson and Martial Hebert. Using Spin Images for Efficient Object Recognition in Cluttered 3D Scenes. *IEEE Transactions on pattern analysis and machine intelligence*, 21(5):433–449, 1999.
- [19] Giseop Kim and Ayoung Kim. Scan Context: Egocentric Spatial Descriptor for Place Recognition within 3D Point Cloud Map. In *2018 IEEE/RSJ International Conference on Intelligent Robots and Systems (IROS)*, pages 4802–4809. IEEE, 2018.
- [20] Will Maddern, Geoffrey Pascoe, Chris Linegar, and Paul Newman. 1 Year, 1000km: The Oxford RobotCar Dataset. *The International Journal of Robotics Research*, 36(1):3–15, 2017.

- [21] Martin Magnusson. *The Three-Dimensional Normal-Distributions Transform: An Efficient Representation For Registration, Surface Analysis, and Loop Detection*. PhD thesis, Örebro universitet, 2009.
- [22] Jiawei Mo and Junaed Sattar. Extending Monocular Visual Odometry to Stereo Camera System by Scale Optimization. In *Proceedings of the IEEE/RSJ International Conference on Intelligent Robots and Systems (IROS)*. To appear, November 2019. arXiv preprint arXiv:1905.12723.
- [23] Raul Mur-Artal and Juan D Tardós. ORB-SLAM2: An Open-Source SLAM System for Monocular, Stereo and RGB-D Cameras. *IEEE Transactions on Robotics*, 33(5):1255–1262, 2017.
- [24] Aude Oliva and Antonio Torralba. Building the Gist of a Scene: The Role of Global Image Features in Recognition. *Progress in brain research*, 155:23–36, 2006.
- [25] Florent Perronnin and Christopher Dance. Fisher Kernels on Visual Vocabularies for Image Categorization. In *2007 IEEE Conference on Computer Vision & Pattern Recognition*, pages 1–8. IEEE, 2007.
- [26] Ethan Rublee, Vincent Rabaud, Kurt Konolige, and Gary R Bradski. ORB: An Efficient Alternative to SIFT or SURF. In *ICCV*, volume 11, page 2. Citeseer, 2011.
- [27] Federico Tombari, Samuele Salti, and Luigi Di Stefano. Unique Signatures of Histograms for Local Surface Description. In *European Conference on Computer Vision*, pages 356–369. Springer, 2010.
- [28] Federico Tombari, Samuele Salti, and Luigi Di Stefano. A Combined Texture-Shape Descriptor for Enhanced 3D Feature Matching. In *2011 18th IEEE international conference on image processing*, pages 809–812. IEEE, 2011.
- [29] Yawei Ye, Titus Cieslewski, Antonio Loquercio, and Davide Scaramuzza. Place Recognition in Semi-Dense Maps: Geometric and Learning-Based Approaches. In *Proc. Brit. Mach. Vis. Conf.*, pages 72–1, 2017.